Interface materials for organic solar cells†

Roland Steim,*[ab] F. René Kogler[a] and Christoph J. Brabec[cd]

Received 19th October 2009, Accepted 26th January 2010
First published as an Advance Article on the web 15th February 2010
DOI: 10.1039/b921624c

The progress in the development and understanding of interfacial materials for organic photovoltaics (OPV) is reviewed. The proper choice of interface materials is a must for highly efficient and stable OPV devices and has become a significant part of the OPV research today. Interface materials are either non-conducting, semiconducting or conducting layers which not only provide selective contacts for carriers of one sort, but can also determine the polarity of OPV devices, affect the open-circuit voltage, and act as optical spacers or protective layers. In this review both inorganic and organic interface materials are discussed with respect to their function in the OPV device.

1 Introduction to OPV

Power conversion efficiencies (PCE) of organic photovoltaic (OPV)[1–3] cells have been increasing continuously over the last few years and reached 6–8%[4–6] for the normal (substrate/hole selective contact/active layer/electron selective contact) and 3–4%[7,8] for the inverted (substrate/electron selective contact/active layer/hole selective contact) structure. Combined with increased lifetime,[10] low weight, low cost production and flexibility this technology is getting more and more attractive as an independent energy source.[11] The improvements in device performances are strongly related to improved processing conditions, but also on the use of novel acceptor,[12] donor[13–15] and interface[16,8] materials. The PCE of a solar cell is defined as: $PCE = Jsc \times Voc \times FF/P_{in}$ (where Jsc is the short-circuit current density, Voc is the open-circuit voltage, FF is the electrical fill-factor and P_{in} is the incident optical power density). The continuous improvement of these parameters (Jsc, Voc and FF) results in the reported efficiencies. Beside the development and synthesis of novel and improved donors and acceptors, the engineering of improved interface materials is of importance for highly efficient and stable OPV devices and modules, since unadjusted interfaces limit or even drastically reduce the PCE.

Table 1 illustrates the importance of the right choice of the interfacial material. For the same active layer, *i.e.* blend of poly(3-hexylthiophene) (P3HT) : [6,6]-phenyl C61 butyric acid methyl ester (PCBM), but varying interfacial layers the PCE, Jsc, Voc and FF are summarized for the inverted structure.

In the first part of this review the functions of interfacial layers as well as the general concepts of OPV such as contact formation and band alignment between two layers are summarized. In the second part an overview of materials is presented including metals, dipole layers, n- and p-type organic and inorganic

[a]*Konarka Technologies GmbH, Landgrabenstr. 94, D-90443 Nürnberg, Germany. E-mail: rsteim@konarka.com*
[b]*Light Technology Institute, University of Karlsruhe (TH), Kaiserstr. 12, D-76131 Karlsruhe, Germany*
[c]*Institute of Materials for Electronics and Energy Technology, University of Erlangen, Martensstr. 7, D-91058 Erlangen, Germany*
[d]*ZAE Bavaria, Am Weichselgarten 7, D-91058 Tennenlohe, Erlangen, Germany*
† This paper is part of a themed issue of *Journal of Materials Chemistry* on Interface engineering of organic and molecular electronics, guest edited by Alex Jen.

Roland Steim

Roland Steim received his Masters of Science degree in Electrical Engineering in 2006 from the University of Karlsruhe. The subjects of his thesis were optical technologies and organic electronics. Since 2007 he has been pursuing his PhD work at the University of Karlsruhe in cooperation with Konarka, Germany, which is expected to be finished in 2010. His research includes the improvement of interface materials for organic solar cells and failure analysis of solar modules during accelerated lifetime testing.

F. René Kogler

René Kogler studied chemistry at the University of Vienna and received his PhD in materials chemistry from the Vienna University of Technology in 2006. During a postdoctoral stay at Cornell University he first got in touch with organic photovoltaics (OPV) and joined the German R&D headquarters of Konarka in 2008 where he is now leading the interface and packaging activities. His research focuses on the development of concepts for improving the lifetime of OPV modules.

Table 1 Summary of relevant improvements in device performance for the inverted device structure. Reference 18 is measured at 130 mW cm^{-2}, all others at 100 mW cm^{-2}. Adapted with permission from ref. 17. Copyright 2009, Wiley VCH

Device structure	Jsc/mA cm^{-2}	Voc/V	FF [%]	PCE [%]	Reference
ITO/Cs_2CO_3/P3HT:PCBM/V_2O_5/Al	8.42	0.56	62.1	2.25	18
ITO/ZnO/P3HT:PCBM/Ag	11.22	0.556	47.5	2.58	85
ITO/TiOx/P3HT:PCBM/Pedot:PSS/Au	9.0	0.56	62	3.1	83
ITO/PTE/TiOx/P3HT:PCBM/Pedot:PSS/Ag	10.2	0.56	64	3.6	80
ITO/ZnO NP/P3HT:PCBM/Pedot:PSS/Ag	11.17	0.623	54.3	3.3	87
FTO/TiO_2/P3HT:PCBM/Pedot:PSS/Au	12.40	0.641	51.1	4.07	7
ITO/annealed Cs_2CO_3/P3HT:PCBM/V_2O_5/Al	11.13	0.59	63	4.19	76

materials. In some parts, materials and results from organic light emitting diodes (OLEDs) are added.

2 Function of interfacial layers

A fundamental difference of OPV compared with inorganic photovoltaic materials is the creation of strongly bound electron–hole pairs (excitons) upon absorption of light in the organic semiconducting materials. The energy which is required to split an exciton is in the range of 100–400 meV compared to a few meV for crystalline semiconductors. The thermal energy kT at standard conditions and the electric field is not sufficient to dissociate these excitons.[19] In order to split excitons into free charge carriers, the energy can be provided in the presence of an electron accepting material with a different electron affinity than the donor material. A typical organic semiconducting material system which enables effective exciton splitting is P3HT and PCBM. Since the diffusion length of excitons is typically in the range of 1–10 nm,[19] the limiting process is the diffusion of the exciton towards a donor–acceptor interface where it is split into charge carriers. A bilayer device of acceptor and donor is thus strongly limited to the diffusion length of excitons. Therefore, the thickness of the photoactive layer is thin for a bilayer device. Blending of donor and acceptor material followed by deposition onto a substrate can result in a bulk-heterojunction device structure. The bulk-heterojunction is not only a random mixture of two materials but consists of homogeneously distributed acceptor and donor phases with appropriate dimensions to effectively split excitons in the whole bulk. An exciton is split into free carriers at the donor/acceptor interface and the free carriers are transported *via* percolated donor and acceptor pathways to the corresponding electrode, *i.e.* electrons by the acceptor to the electron selective contact and holes by the donor to the hole selective contact. In this review the hole selective contact is named anode and the electron selective contact is named cathode. The thickness limiting factor of this configuration is then the mobility–lifetime product of the photo-generated carriers. The fundamental processes from light harvesting to power generation can be summarized as follows:

(a) Light is absorbed by the donor, *e.g.* P3HT, and excitons are created. Absorption by the acceptor is neglected in this description.

(b) Excitons diffuse to the donor–acceptor interface and are split into free carriers.

(c) The carriers are transported to the respective electrode, electrons by the acceptor to the cathode and holes by the donor to the anode.

(d) Interfacial layers enable the unipolar extraction of photo-generated carriers from the photoactive layer to the electrodes.

A schematic illustration of a solar cell under operation, *i.e.* in extraction mode, is shown in Fig. 1.

The interface which is formed between the photoactive layer and the electrodes is essential for highly efficient and stable OPV devices. The main functions of interface materials are:

(1) to adjust the energetic barrier height between the active layer and the electrodes

(2) to form a selective contact for carriers of one sort

(3) to determine the polarity of the device

(4) to prohibit a chemical or physical reaction between the polymer and electrode

(5) to act as optical spacer.

To discuss the different functions of interfacial layers, an understanding of contact formation between the active layer, the interfacial layers and the electrode materials is required. Therefore, section 2.1 gives a short introduction to the contact formation between different materials. In sections 2.2–2.7 the function of interfacial layers is discussed in detail.

2.1 Theory of contact formation active layer/interfacial layer

Interface materials are applied between the photoactive layer, *i.e.* donor and acceptor materials, and the electrode materials. The understanding of the function of those interfacial layers, *i.e.*

Christoph J. Brabec

Christoph J. Brabec holds the chair "materials for electronics and energy technology (i-MEET)" at the materials science institute of the Friedrich Alexander University Erlangen-Nürnberg, and is scientific director of the Erlangen division of the Bavarian research institute for renewable energy. He received his PhD (1995) in physical chemistry from Linz University, joined Prof. Alan Heeger at UCSB for a sabbatical, worked on organic semiconductor spectroscopy as assistant professor at Linz with Prof. Serdar Sariciftci, joined the SIEMENS research labs as project leader for organic semiconductor devices in 2001 and joined Konarka in 2004, where he was CTO before joining university.

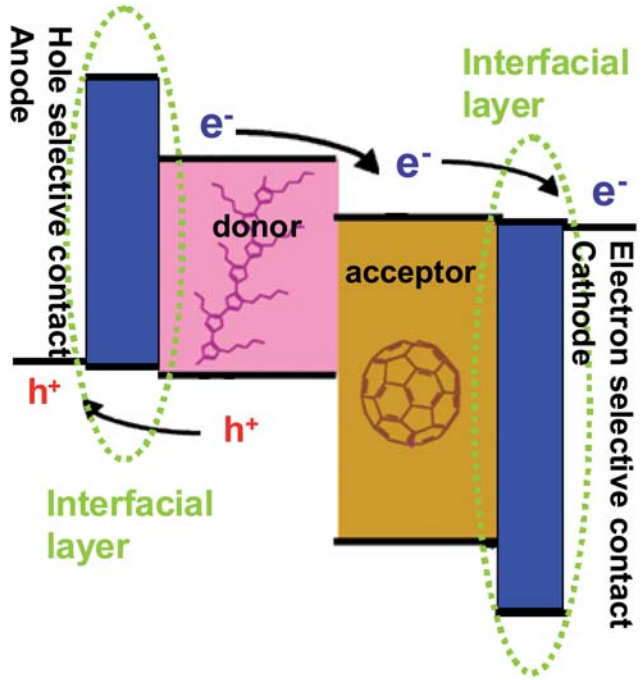

Fig. 1 Schematic illustration of an organic solar cell in extraction mode. Excitons are created and diffuse to the donor/acceptor interface where the excitons are split. The charge carriers are transported to the electrodes and are extracted by the interfacial layers to the respective electrode.

metals, metal like, organic materials and combinations thereof, and the resulting band alignment between electrode–interfacial layer–active layer is essential for the proper choice of such interfacial materials. The integer charge model was developed for OPV devices and found to be valuable for most interfaces which are relevant to OPV.[21,22] This theory predicts Fermi level pinning of a conducting interfacial layer to the organic semiconductor until equilibrium is reached when spontaneous charge transfer between these two layers is possible. In the case of no charge transfer between the two layers, no Fermi level pinning takes place.

Fig. 2 presents experimental results on the energy level alignment between the low-band-gap polymer polyfluorene APFO-Green1 coated on a conducting substrate. The substrate work function was varied between 3.0 eV and 5.5 eV and the resulting band alignment was then measured when APFO-Green1 was coated on the substrate. In this review we compare the absolute values of the work function. For substrate work functions larger than 4.6 eV and lower than 3.6 eV, the Fermi level of the substrate is pinned to APFO-Green1, *i.e.* to 3.6 eV and 4.6 eV, respectively. In the integer charge model these states are called positive (E_{ICT+}) and negative (E_{ICT-}) integer charge-transfer states. E_{ICT+} is defined as the energy which is required to extract one electron from the polymer/molecule to produce a thermally fully relaxed state. E_{ICT-} is defined as the energy which is gained when one electron is added to the molecule/polymer in order to produce a fully relaxed state. These states differ from the lowest unoccupied molecular orbital (LUMO) and highest occupied molecular orbital (HOMO) of the organic semiconductor. In between these states a linear correlation between the substrate

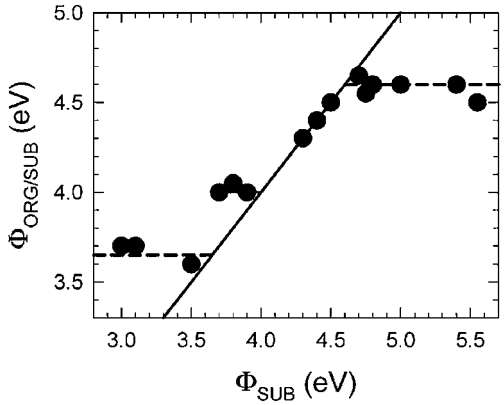

Fig. 2 Dependence of the work function of molecule-coated substrates ($\Phi_{org/sub}$) on the work function of bare substrates (Φ_{sub}) for APFO-Green1.[21] The solid line is added as a guide to the eye, illustrating the slope = 1 dependence as expected for vacuum level alignment. The dashed lines are added as guides to the eye, illustrating the slope = 0 dependence expected for a Fermi-level pinned interface. Adapted with permission from ref. 22. Copyright 2009, Wiley VCH.

work function (Φ_{sub}) and the measured work function organic/substrate ($\Phi_{org/sub}$) with a slope of 1 was found. The system describes a full "Mark of Zorro" dependence. The Fermi level pinning of the conducting substrate to the charge transfer states was also observed experimentally for several other organic semiconductors and fullerenes, including P3HT and C_{60}.[20,22]

The "Mark of Zorro" dependence is schematically depicted in Fig. 2 and described in the integer charge model as follows. Depending on the position of the substrate or electrode Fermi level relative to E_{ICT+} and E_{ICT-}, three scenarios can be distinguished which are schematically depicted in Fig. 3:

(a) When the substrate work function is larger than E_{ICT+} of the polymer, electrons will flow from the polymer to the substrate and the Fermi level of the substrate will be pinned to E_{ICT+} of the polymer.

(b) When the Fermi level of the substrate is in between E_{ICT+} and E_{ICT-}, no Fermi level pinning occurs.

(c) When the substrate work function is smaller than E_{ICT-} of the polymer, electrons will flow from the substrate to E_{ICT-} of the polymer and the Fermi level of the substrate will be pinned to E_{ICT-} of the polymer.[22]

Analogously, the integer charge model can be transferred to stacked multilayer systems. A more detailed description of this model including physisorption, chemisorption and the induced density of states model is given in the review of Braun *et al.*[22] and other reports.[23–25]

2.2 Impact on the open-circuit voltage

Interface materials enable the electrical contact between the active layer and the electrode materials for charge carrier extraction. As such, the impact of the interfacial layers on Voc of a device needs to be investigated more closely. Two models were discussed extensively in the literature. The Metal–Insulator–Metal (MIM) model describes that Voc originates from the work function difference of the electrode materials. This model is applied for non-ohmic contacts where no Fermi level pinning between cathode–donor and anode–acceptor occurs. Mihailetchi

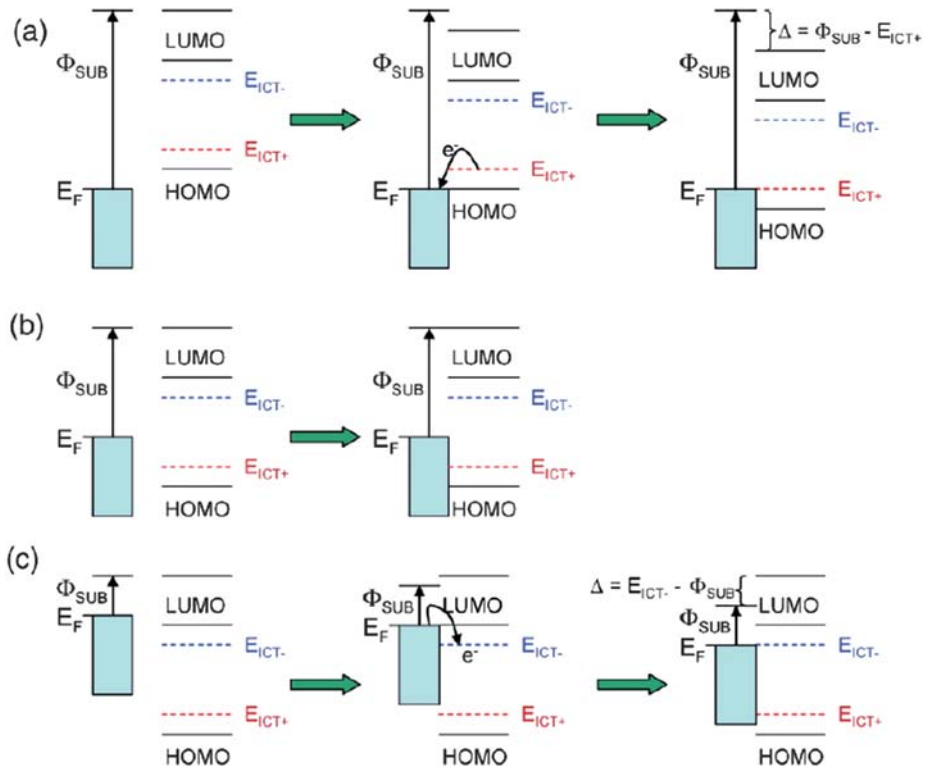

Fig. 3 Schematic illustration of the evolution of the energy-level alignment when a π-conjugated organic molecule or polymer is physisorbed on a substrate surface when a) $\Phi_{sub} > E_{ICT+}$: Fermi-level pinning to a positive integer charge-transfer state, b) $E_{ICT-} < \Phi_{sub} < E_{ICT+}$: vacuum level alignment, and c) $\Phi_{sub} < E_{ICT-}$: Fermi-level pinning to a negative integer charge-transfer state. The charge-transfer-induced shift in vacuum level, Δ, is shown where applicable. Adapted with permission from ref. 22. Copyright 2009, Wiley VCH.

et al. reported that for non-ohmic contacts Voc is determined by the work function difference of the electrodes. The cathode materials were varied while the anode material in all experiments was ITO/poly(3,4-ethylenedioxythiophene) poly(styrene-sulfonate) (Pedot:PSS). Voc is reduced from 0.59 V for Ag to 0.398 V for Pd as cathode material, compared to a difference in the work function of the investigated cathodes of 0.29 V. In this regime Voc correlates linearly with the work function differences of the investigated cathodes with a scaling factor close to 1. The scaling factor is defined as the quotient of the difference of Voc and the difference of the work functions for the investigated cathode materials. Pd forms a non-ohmic contact to [6,6]-phenyl C61-butyric acid methyl ester (PCBM).[26]

For ohmic contacts the situation is different. In section 2.1 it was discussed that Fermi level pinning occurs when the substrate work function exceeds E_{ICT+} and is below E_{ICT-}, respectively. These results have been experimentally confirmed for P3HT and C60, the fruit fly semiconductors for OPV. The relevant interfaces are anode–donor and cathode–acceptor because electrons are transported by the acceptor and holes by the donor material in OPV cells. Therefore, E_{ICT+}, E_{ICT-} and the respective band alignment at the interfaces formed between semiconducting polymer/interfacial layer/electrode are relevant for the open-circuit voltage of the OPV device. Thus, the highest possible open-circuit voltage is the difference of E_{ICT+} of the donor and E_{ICT-} of the acceptor, independent of the work function of the interfacial material, provided that Fermi level pinning occurs. Interfacial materials with a Fermi level located between E_{ICT+} and E_{ICT-} reduce the Voc. For instance, the origin of Voc was investigated in detail for poly(2-methoxy-5-(3′,7′-dimethylocty-loxy)-1,4-phenylenevinylene) (MDMO-PPV) blended with highly soluble fullerene derivatives as active layer. The investigated structure was ITO/Pedot:PSS/MDMO-PPV:Fullerene/metal electrode with the fullerene and the electrode as varying parameters. The work function of the metal electrode, *i.e.* cathode, was varied from 5.1 eV for Au to 2.87 eV for Ca/Ag. This resulted in an increase of Voc from 0.650 V to 0.814 V. The corresponding scaling factor was estimated as 0.1 or lower (Fig. 4). This contact behavior is explained by the Fermi level pinning mechanisms which occur for ohmic contacts. In contrast, for non-ohmic contacts it was found that the Voc is influenced by the work function of the interface materials, see palladium above.[26]

In another experiment the LUMO of the acceptor was varied and the influence of Voc was investigated. It was found that a decrease of the LUMO of the acceptor by 160 mV (reduction potential changed from −0.53 V for N-3-[2-ethylhexyloxy]benzyl ketolactam to −0.69 V for PCBM *vs.* normal hydrogen electrode) increases Voc from 0.56 V to 0.76 V. The corresponding scaling factor is close to 1 and proves that Voc is controlled by the LUMO of the acceptor as depicted in Fig. 4.[27]

Fig. 5 illustrates experimental results on the dependence of the Voc to the HOMO position of the donor polymer, *i.e.* the onset of oxidation, for 26 donors. The linear fit of the measured points has a slope equal to 1 which proves that Voc correlates linearly with the HOMO of the donor.[28]

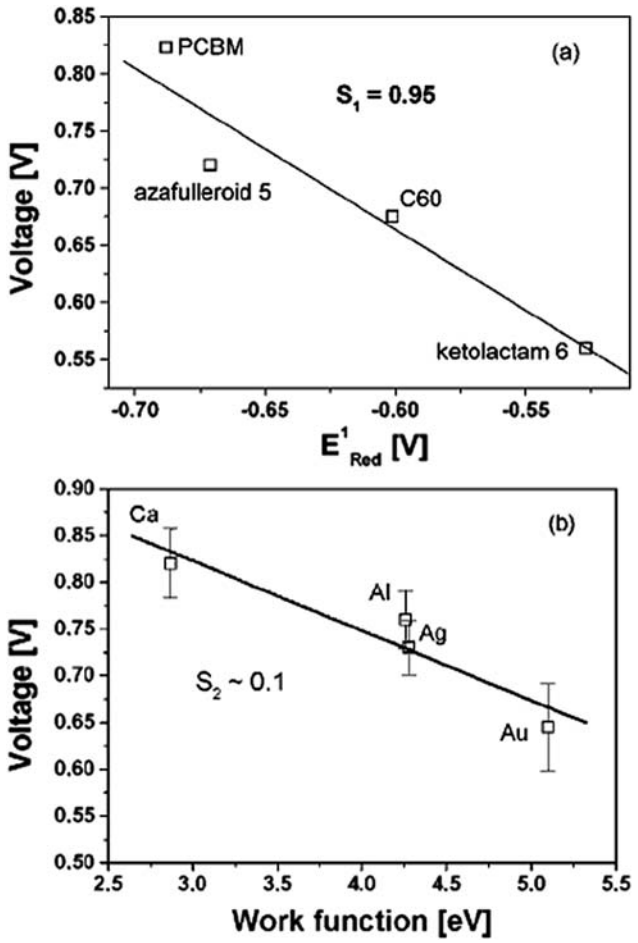

Fig. 4 a) Voc *versus* acceptor strength and b) Voc *versus* electrode work function. The slopes S1 and S2 of the linear fits of the experimental data are given inside the figures. Adapted with permission from ref. 27. Copyright 2001, Wiley VCH.

In conclusion Voc correlates with the HOMO of the donor and the LUMO of the acceptor in the case of ohmic contacts—the Fermi levels of the interfacial and electrode materials are pinned to E_{ICT+} of the donor at the anode and E_{ICT-} of the acceptor at the cathode. For non-ohmic contacts Voc is influenced by the interface materials—the upper limit of Voc is the difference of E_{ICT+} of the donor and E_{ICT-} of the acceptor.[29] Voc values exceeding these limits have not been observed to the best of our knowledge.

2.3 Determination of the polarity of the device

Two different geometries of OPV cells, the normal and the inverted structure, are reported in the literature (Fig. 6), depending on whether the bottom electrode forms the anode or the cathode. The bottom electrode is the transparent electrode, *e.g.* ITO, on which the OPV cell is constructed. In the normal structure holes are extracted at the bottom electrode, in the inverted structure holes are extracted at the top electrode. The active layer of an OPV cell in many cases is formed by a bulk-heterojunction where the donor and an acceptor material are blended. In an ideal case the donor and acceptor materials are distributed equally throughout the active layer. Therefore,

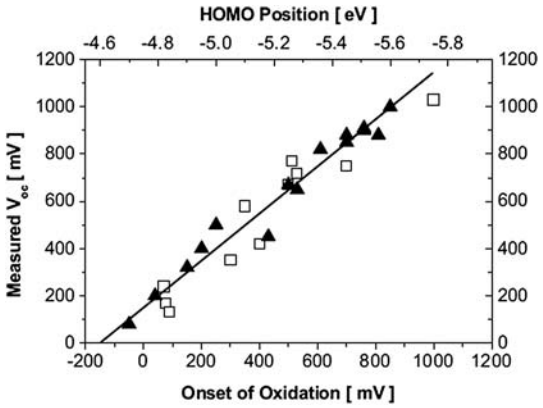

Fig. 5 Voc of different bulk-heterojunction solar cells plotted *versus* the oxidation potential/HOMO position of the donor polymer used in each individual device. The straight line represents a linear fit with a slope of 1. Adapted with permission from ref. 28. Copyright 2006, Wiley VCH.

a bulk-heterojunction does not have a preferential direction to extract electrons or holes to one side of the solar cell. The interface materials/electrodes which are sandwiching the active layer constitute the cathode and the anode of the OPV cell, *i.e.* the interfacial layer/cathode with the larger work function forms the anode. Depending on the thickness and type of the used interface materials, the polarity of the device may become independent of the used electrode materials. For instance, Pedot:PSS and TiOx (titanium oxide) are utilized in the normal as well as in the inverted structure. TiOx determines the cathode and Pedot:PSS the anode of an OPV cell, independent of the used electrode materials (see Fig. 6).

Fig. 7 presents the J-V characteristics of devices in the normal structure (ITO/Pedot:PSS/P3HT:PCBM/LiF/Al) and inverted structure (ITO/TiOx/P3HT:PCBM/Pedot:PSS/Au). In both devices Pedot:PSS is used as the anode material, the cathode, however, is either given by the LiF/Al contact or by the ITO/TiOx layer. Both architectures give quite comparable performance, the differences in device performance are usually explained with a vertical phase separation[30,31] of the acceptor and donor, which may be more favorable for one structure *versus* the other, but not sufficient to determine the polarity of the OPV device.[32]

2.4 Electrode materials—conductive layers

Some interfacial layers act as both interfacial layer and electrode material. A low sheet resistance of electrode materials (<10 Ω/sq)

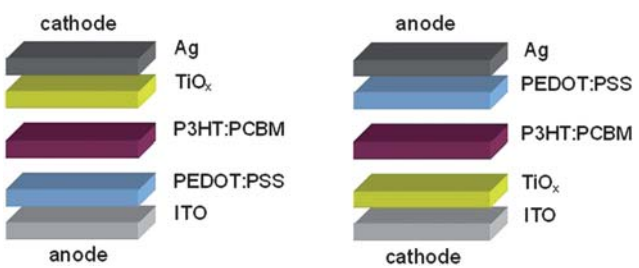

Fig. 6 Device structure in the normal (left) and inverted structure (right).

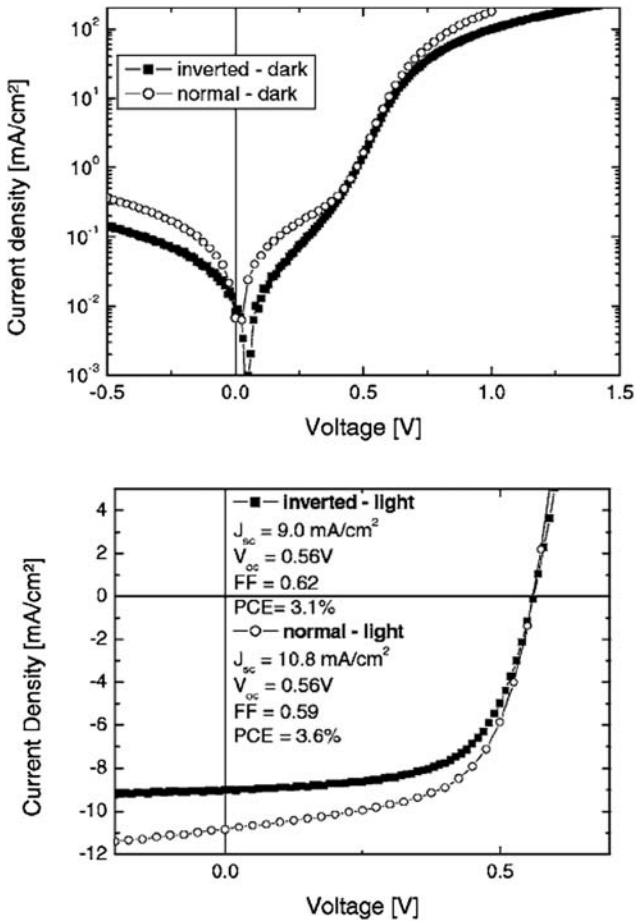

Fig. 7 J-V curves in a semilogarithmic representation for the normal (open circles) and inverted (solid squares) OPV in the dark (upper plot) and under illumination (bottom plot). Adapted with permission from ref. 32. Copyright 2006 American Institute of Physics.

is essential to transport the photo-generated carriers with little losses. Many metals are typically utilized for the non-transparent back contact. The materials for the transparent front electrodes are much more limited. Indium tin oxide (ITO) is the most prominent transparent electrode for OPV devices. ITO provides sufficiently high transmittance (~90%) and low sheet resistance (~10 Ω/sq). ZnO doped with group III elements, *i.e.* B,[33] Ga[34–36] and Al[37,38] are alternative transparent electrode materials. Other approaches to replace ITO are carbon nanotubes,[39] graphene,[40] highly conductive polymers,[41] metal grids,[42] metal nano-meshes,[43] optically thin metal layers alone[44] or thin metals in combination with other metal oxides.[45]

2.5 Optical spacer

Most OPV devices consist of a transparent front electrode and a non-transparent reflecting back electrode. Light enters the OPV cell through the transparent electrode and is reflected at the non-transparent electrode. Therefore, the light passes the active layer twice and a standing wave is formed, with the electrical field strength $|E| = 0$ at the reflecting electrode and its maximum somewhere in the bulk, depending on the refractive index and the thicknesses of the layers. The absorption of light depends on the electrical field strength of the light which depends on the phase. For OPV cells with a photoactive layer thickness in the range of 100 nm, interference effects may become important. The absorbing active layer thickness needs to be correlated to the mobility-lifetime product of photo-generated carriers within the active layer, so that most photo-generated charge carriers can reach the electrodes. The optical spacer effect is a concept to optimize the absorption within the active layer. A transparent layer is inserted between the reflecting electrode and the active layer. Depending on the thickness and refractive index of the transparent optical spacer layer, the absorption maximum can be shifted. A layer thickness of a few tens of nm might be enough to improve the absorption within the active layer significantly. Once optimized, such an optical spacer layer can help to improve the short-circuit current of an OPV device, specifically for thin film devices which otherwise would not absorb all light in a single pass.[46] An example of an OPV cell structure with and without optical spacer is glass/ITO/PEDOT/P3HT:PCBM/TiOx/Al and is given in Fig. 8. Here, TiOx acts as optical spacer.[47–49]

2.6 Protective layer between polymer and electrode

An interfacial layer protects the organic layer from physical or chemical interaction with the electrode materials. For example, metals are often used as electrode material providing the conductivity needed to extract photo-generated carriers. The diffusion of metal atoms into polymeric layers during the thermal evaporation process causes shunting or electrical shorting of the organic devices and limits their lifetime.[50–52] The protection of the active layer from oxygen and water of the atmosphere by an interfacial layer of TiOx is also reported as an interesting approach to improve lifetime.[53]

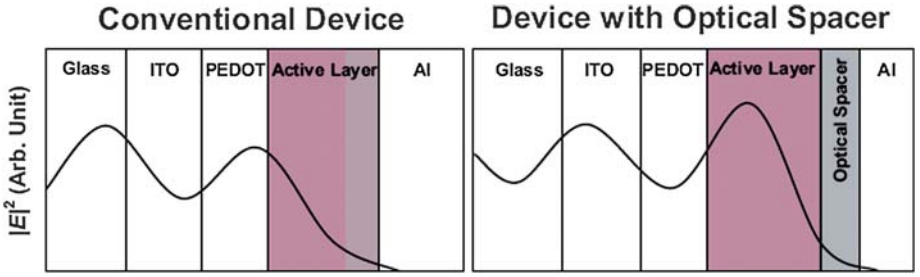

Fig. 8 Schematic representation of the spatial distribution of the squared optical electric field strength $|E|^2$ inside the devices with a structure of ITO/PEDOT/active layer/Al (left) and ITO/PEDOT/active layer/optical spacer/Al (right). Adapted with permission from ref. 47. Copyright 2006, Wiley VCH.

2.7 Selective contact for carriers of one sort and exciton blocking layer

Since excitons and carriers are created in the entire active layer, interfacial layers form selective contacts and prevent excitons and carriers from recombining at the electrodes.[54–58] Thus, interfacial layers form a barrier for carriers of one sort, and pass by the carriers of the opposite sort. For instance, the cathode enables or facilitates extraction and injection of electrons, but blocks holes. Interfacial layers which act as an exciton blocking layer have a bandgap higher than the one of the acceptor and donor of the active layer. The transfer of excitons through the interfacial layer is not possible without a supply of additional energy. Therefore, an interfacial layer can act as an exciton blocking layer.

3 A material overview of interfacial layers

Some materials discussed in this review can be used as both electrode material and interfacial layer. Other materials, *e.g.* when the conductivity is not sufficient, are sole interface materials. In the following the most prominent interface materials will be reviewed, categorized as conducting layers, semiconducting layers and interface dipole layers. Also we will distinguish between cathode (n-type) and anode (p-type) materials.

In organic electronics it was demonstrated that chemical doping with organic and inorganic materials can modify material properties such as conductivity and the Fermi level.[59–63] For efficient n-type doping the HOMO level of the dopant or Fermi level must be lower than the LUMO level of the material that has to be doped. For p-type doping the LUMO level of the dopant has to be higher than the HOMO level of the material to be doped.

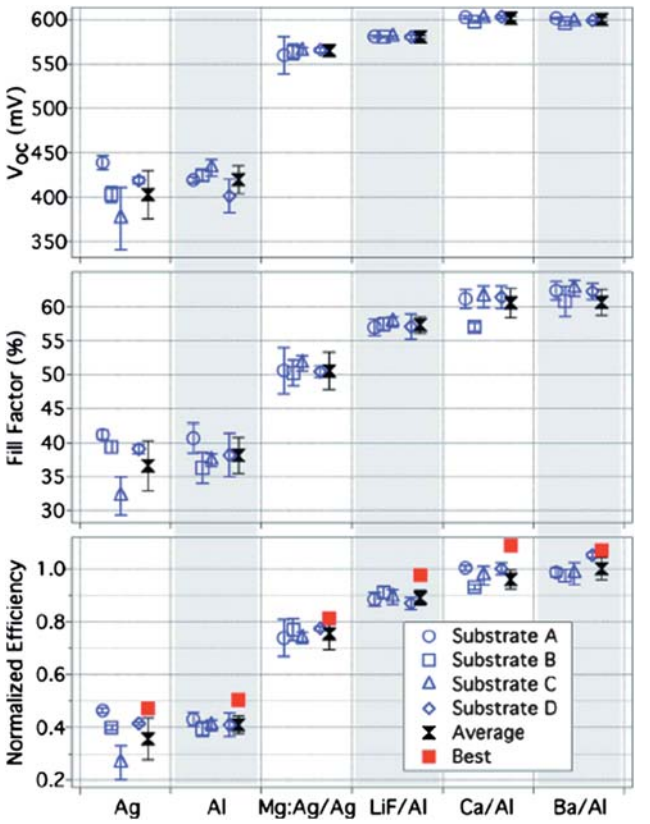

Fig. 9 Voc, FF, and normalized efficiency *vs.* negative electrode type. Average values are displayed both for individual and groups of substrates. Error bars denote plus and minus one standard deviation. "Best" efficiency values are for devices made by Reese *et al.* Adapted with permission from ref. 66. Copyright 2008 American Institute of Physics.

3.1 Metals

Metals can be thermally evaporated in optical thick and thin layers to form a non-transparent or transparent electrode or/and interfacial layer. Especially for Ag which is widely used, several deposition methods have been successfully demonstrated. For instance, spray-coating of Ag nanoparticles,[64] Ag pastes and transparent Ag nanowire meshes[65] have been reported to be feasible for solution processing, which makes these materials attractive for roll-to-roll printing processes.

Al, Mg/Ag, Ca/Al, Ca/Ag, Ba/Al,Au, Ti were successfully used in OPV devices.[66] A combination of a low work function metal (Ca, Ba) with Ag or Al is a common way to decrease the work function of the electrode and to prevent Ag and Al atoms from diffusing into the polymeric layer. The work function of these metals ranges from 5.1 eV for Au[67] to 2.7 for Ba.[67] Fig. 9 illustrates experimental results for several electrode materials as cathodes in the normal device structure (ITO/PEDOT:PSS/P3HT:PCBM/cathode). Voc, FF and the normalized efficiency is depicted. The pristine metals Al and Ag have the lowest performance while in combination with Mg : Ag, LiF, Ba or Ca the device performance is clearly improved because these materials decrease the work function of the cathode, act as protection layer and improve the selectivity.

Apart from a modification of the work function of the electrode and physical barrier layer, low work function metals have also been used to n-dope organic layers. This is possible when the work function of the metal is smaller than the LUMO of the organic layer, *e.g.* Mg can dope C_{60}.[68] Fig. 10 gives a comprehensive overview of the work functions of metals and semimetals.[69,67]

3.2 Semiconducting layers

Many semiconducting interfacial materials were shown to be feasible for OPV applications. We distinguish between inorganic materials (metal oxides) and organic materials, reviewing the most prominent ones. Transparency, *i.e.* little absorption losses, is a must for efficient OPV devices and allows the deposition of thick layers without absorption losses. As such, interfacial materials are often required to be transparent in the visible light spectrum. Moreover, doped semiconducting materials with a high conductivity can be used as transparent electrode material and thick interfacial layers.

3.2.1 Inorganic materials–metal oxides. Metal oxides can be p-type and n-type materials, depending on the position of the valence band and conduction band. For a p-type contact material, the valence band of the metal oxide is required to match the HOMO of the polymer. For an n-type material, electron transfer from the LUMO of the acceptor to the conduction band of the

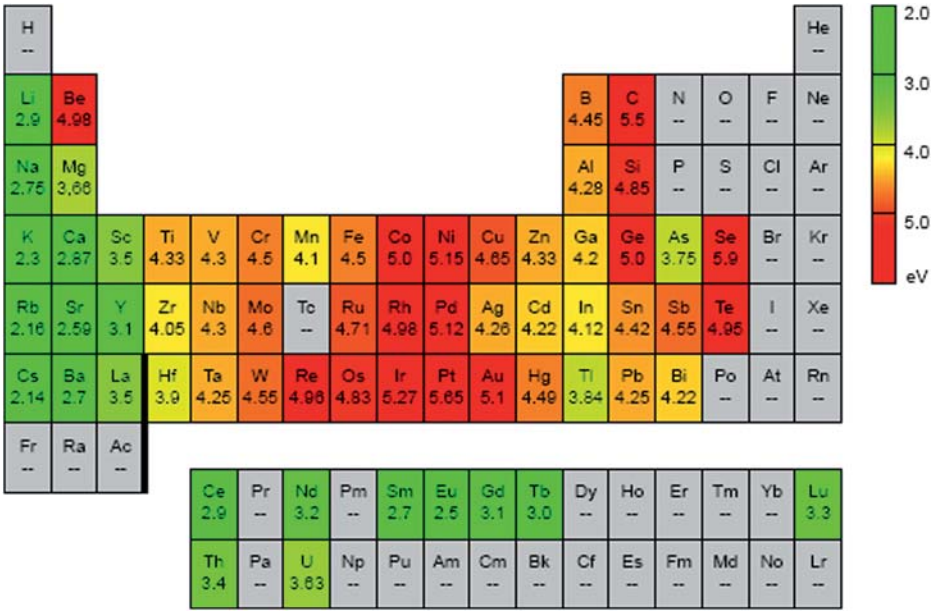

Fig. 10 Work function of the elementary solids.[69] Adapted with permission from ref. 67. Copyright 1977 American Institute of Physics.

metal oxide is required. A wide band gap of the interface material then results in a barrier for carriers of the other sort and enables highly selective contacts. Fig. 11 summarizes widely used p-type and n-type metal oxides for the P3HT-PCBM donor–acceptor system. As reference, the energetic level of the most common interface material Pedot:PSS is added.

3.2.1.1 p-Type inorganic materials. p-Type like transition metal oxides have been successfully introduced in OPV. WO_3,[70–72] NiO,[54] V_2O_5[73–76] and MoO_3[73,77] are such p-type like metal oxides with respect to P3HT. Shrotriya *et al.*[73] demonstrated that thermally evaporated transition metal oxides have the potential to replace Pedot:PSS. They studied different layer thicknesses of V_2O_5 and MoO_3 and compared results of OPV devices without and with Pedot:PSS as p-type interfacial layer (Table 2).

A clear improvement in Jsc, Voc, FF and PCE is observed for all investigated metal oxide layer thicknesses compared to OPV devices without p-type interfacial layer (ITO only). Thin layers of metal oxide (1nm) do not cover the entire electrode; too thick metal oxide layers reduce the Jsc and FF due to the serial resistance of the interfacial oxide. Excellent results are achieved for the optimized layer thickness of V_2O_5 (3nm) and MoO_3 (5 nm).[73] This has been reported for the normal as well as for the inverted structure by various groups.[75,77,78] Moreover, it was shown that stacking of Pedot:PSS with a metal oxide may further improve the device performance.[79]

3.2.1.2 n-Type inorganic materials. TiOx[32,53,80–83] and ZnOx[77,84–87] are well investigated n-type interfacial layers for OPV devices. These materials are transparent in the visible light spectrum but absorb ultraviolet (UV) light. The layer thickness of the interfacial layer is tunable without absorption losses in the visible (VIS) light and thus can additionally act as optical spacer.[47–49]

Fig. 12 illustrates the J-V characteristics of inverted OPV cells with electrodeposited amorphous (TiOx) or anatase (TiO_2) titanium oxide as n-type interfacial layers with and without UV light irradiation. Without UV light irradiation (<440 nm) the PCE of the OPV cell is drastically reduced compared to an OPV cell with

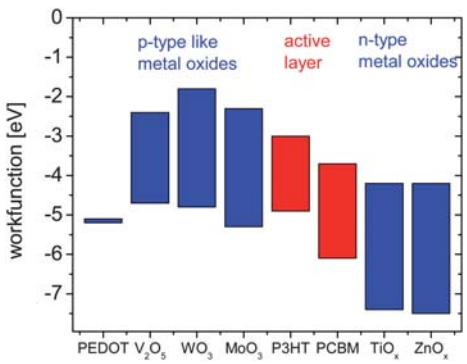

Fig. 11 Energy level diagram of p-type and n-type metal oxides incorporated in OPVs. As references Pedot:PSS, P3HT and PCBM are added. Values are taken from the references given in sections 3.2.1.1 and 3.2.1.2.

Table 2 Device operation parameters for devices with different types of anodes fabricated in this study. Adapted with permission from ref. 73. Copyright 2006 American Institute of Physics

Anode	I_{SC}/mA cm^{-2}	Voc/V	FF (%)	PCE (%)
ITO only	**7.82**	**0.49**	**51.1**	**1.96**
ITO/PEDOT:PSS (25 nm)	**8.95**	**0.59**	**59.6**	**3.18**
ITO/V_2O_5 (1 nm)	8.86	0.59	47.5	2.48
ITO/V_2O_5 (3 nm)	**8.83**	**0.59**	**59.1**	**3.10**
ITO/V_2O_5 (5 nm)	8.54	0.59	57.2	2.88
ITO/V_2O_5 (10 nm)	8.16	0.59	57.9	2.79
ITO/MoO_3 (1 nm)	8.75	0.53	42.3	1.98
ITO/MoO_3 (3 nm)	8.86	0.59	58.3	3.06
ITO/MoO_3 (5 nm)	**8.94**	**0.60**	**61.9**	**3.33**
ITO/MoO_3 (10 nm)	8.73	0.60	59.8	3.13
ITO/MoO_3 (20 nm)	8.19	0.58	59.9	2.86

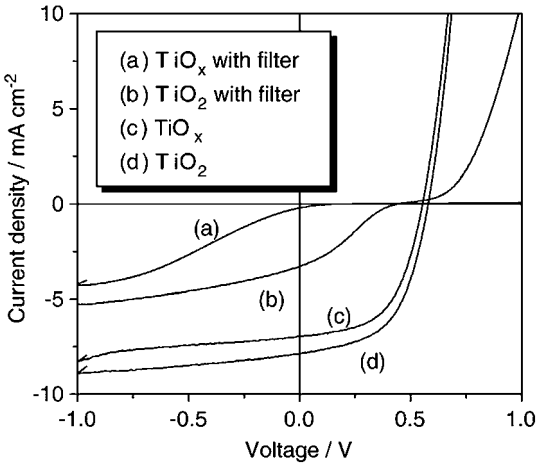

Fig. 12 Photo I–V curves of the FTO/amorphous TiOx/P3HT:PCBM/PEDOT:PSS/Au and FTO/anatase TiO_2/P3HT:PCBM/PEDOT:PSS/Au type solar cells under light irradiation of AM 1.5 100 mW cm^{-2} with and without UV light filter (440 nm). Adapted with permission from ref. 88. Copyright 2008 Elsevier.

UV light irradiation. The PCE with and without UV light irradiation depends on the type of TiOx, amorphous or anatase TiOx. With UV light irradiation the PCE improves to 2.13% for the amorphous TiOx and to 2.48% for the anatase TiO_2 which might be caused by a difference in carrier density.[88]

The design of 3-dimensional structures of metal oxides is another approach to improve the PCE and many groups compare 2-dimensional ZnO layers with 3-dimensional nanostructures.[89–93] The increased interface acceptor/interfacial layer improves the electron transport and is expected to allow for thicker active layers.[94]

Mor *et al.* presented a vertically oriented TiO_2 nanotube film with P3HT:PCBM infiltrated into the nanotubes as illustrated in Fig. 13. PCEs as high as 4.1% were reported in the inverted structure.[95]

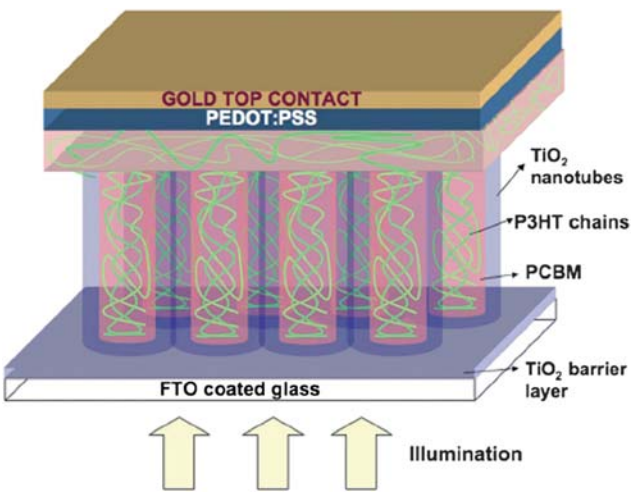

Fig. 13 Illustration showing the device configuration, materials used, and the direction of illumination. Adapted with permission from ref. 95. Copyright 2007 American Institute of Physics.

Another approach for improved PCE is doping of the metal oxide. It was demonstrated that Li_2O doping of TiO_2 improves the conductivity up to 2 orders of magnitude.[96] OPV devices with Cs doped TiO_2 nanocrystals result in a PCE of up to 4.2%, which is one of the highest reported efficiencies for inverted OPV cells based on P3HT:PCBM as active layer to date.[97]

3.2.2 Organic layers. Organic semiconducting layers can be distinguished into polymers and small molecules. Small molecules typically are thermally evaporated, while polymers are solution processed. Solution processing of organic interfacial layers is attractive for cheap and fast roll-to-roll processing. Vacuum steps can be avoided but the downside is that orthogonal solvent systems[98] or cross-linkable polymers have to be used to allow stacking of the individual solution processed layers. p-Type interface materials are hole transport materials which can additionally be p-doped, n-type materials are electron transport materials[99] which can additionally be n-doped. Small molecules have the advantage that the matrix material and the dopant can be co-evaporated. A good review on doping of organic materials for OLEDs and small molecule OPV was done by Walzer *et al.*[100] and shall not be discussed in detail in this review.

3.2.2.1 p-Type organic materials. Pedot (poly(3,4-ethylenedioxythiophene)) is widely used as a solution processed p-type interfacial layer and transparent electrode material in organic electronics. Usually Pedot is doped with PSS (poly(styrene sulfonate)) for improved conductivity and solubility in protic solvents.[101–110] The purpose of the incorporation of Pedot:PSS as p-type interfacial layer is explained in terms of:

- improved selectivity of the anode
- improved smoothness and coverage of *e.g.* ITO peaks
- modified work function of the transparent electrode

Comparable device performances were obtained with alternative organic p-type interfacial layers such as sulfonated poly(diphenylamine),[105,106] polyaniline (PANI)[107,108] and polyaniline-poly(styrene sulfonate) (PANI-PSS).[109]

Fig. 14 summarizes device parameters (Jsc, Voc, FF and PCE) of OPV devices in the normal structure without p-type like interfacial layer and with Pedot:PSS in different thicknesses. All device parameters show a clear improvement when Pedot:PSS is used. Because of good transparency and conductivity the device performance is insensitive to the layer thickness of Pedot:PSS.[110]

Improvements in conductivity of Pedot:PSS reduce losses in the serial resistance which in turn results in increased PCE. This makes the material even more suitable as a transparent electrode material and, results in better performance. For example, mannitol p-dopes Pedot:PSS and improves the conductivity and the performance of OPV devices. An increase in device performance from 4.5% to 5.2% was reported.[111] Additives for Pedot:PSS which improve the conductivity include high-dielectric solvents such as dimethyl sulfoxide and N,N-dimethylformamide, or polar compounds such as glycerol, ethylene glycol, polyalcohols and sorbitol.[112–123] The origin of the improvement in PCE and conductivity is mainly explained with morphological changes. Highly conductive Pedot:PSS which additionally is supported with a metal grid was demonstrated as a transparent electrode in OPV devices.[124–126]

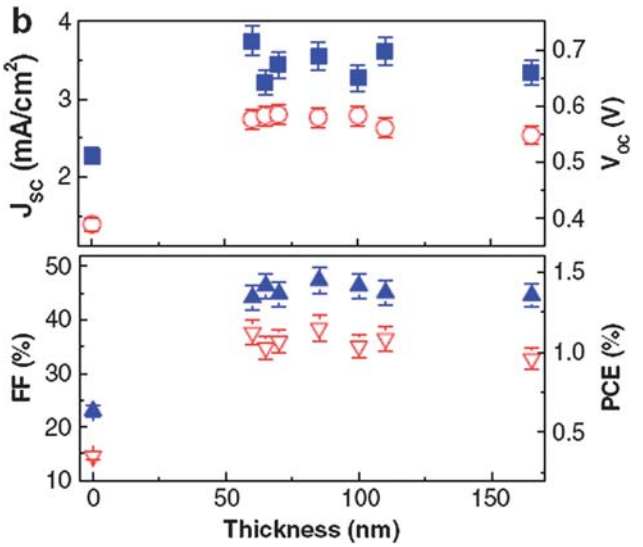

Fig. 14 Jsc (filled squares), Voc (open circles), FF (filled upward triangles), and PCE (open downward triangles) as a function of PEDOT:PSS layer thickness. Adapted with permission from ref. 110. Copyright 2008 Elsevier.

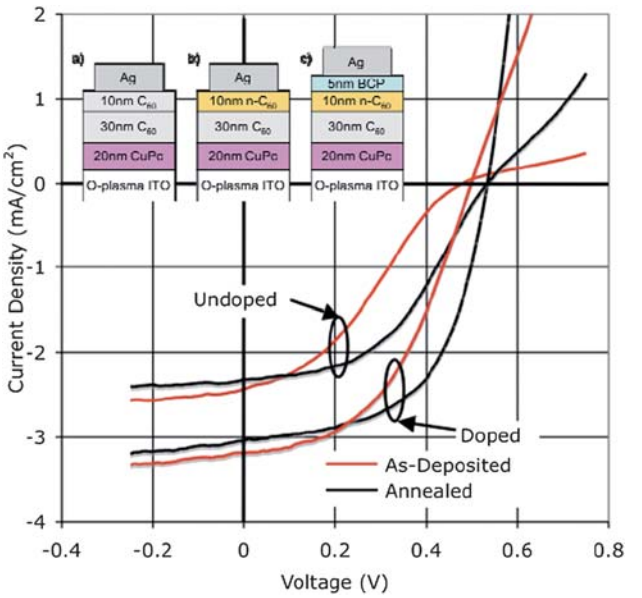

Fig. 15 Current density *vs.* voltage (J-V) characteristics of the diodes under 1 sun illumination. Inset illustrates device structures in this study. "Undoped" data correspond to structure (a) (ITO/phthalocyanine(-CuPc)/C_{60}/Ag). "Doped" data are representative of (b) and (c). Herein C_{60} is doped by $CoCp_2$. Adapted with permission from ref. 141. Copyright 2009 American Institute of Physics.

A major disadvantage of Pedot:PSS is its intrinsic acidity which can cause degradation within the OPV stack. Jong *et al.* studied the interface of Pedot:PSS and ITO by Rutherford backscattering and found that Pedot:PSS etches ITO. Annealing and storage of the sample in air does increase the concentration of indium within Pedot:PSS.[127] A detailed description of other degradation mechanisms is given elsewhere.[128–130]

3.2.2 n-Type organic materials. Little was reported on OPVs with n-type doped organic layers. On the other hand, organic n-type materials are very popular within the OLED community and also within the small molecule OPV community. In this review we will highlight only a few materials and otherwise refer to the excellent review by Walzer *et al.*[100] which also includes the n-type doping of organic layers by alkali metals.

Bathophenanthroline (BPhen)[131] and bathocuproine (BCP) are good electron transport layers and good hole blocking materials.[56,58,132,133] BCP additionally acts as an exciton blocking layer.[56,58] Approaches to n-dope organic materials make use of cationic dyes such as Rhodamine B, Pyronin B, Acridine Orange Base and Leuko Kristall Violett.[134–137] The feasibility of such materials has already been demonstrated for OPV cells.[138,139] The doping of organic materials by metals, *e.g.* the doping of BPhen by ytterbium (Yb), was successfully demonstrated in OPV devices.[140]

Chan *et al.* reported on n-doping of C_{60} with decamethylcobaltocene ($CoCp_2$) in OPV devices[141] and Fig. 15 shows the impact of a doped C_{60} interface layer. FF and Isc could be clearly improved due to the doping of the near contact region.

3.3 Dipole layers

The modification of the work function of the electrode by dipole layers is an elegant alternative way to generate the required interface and to form an Ohmic contact. The surface treatment of electrode materials by dipole layers can result in a modified electrode work function through surface dipole formation. Fig. 16 illustrates the simplest case of acid and base treatment of the electrode material. The arrangement of molecules and charges results in a shift of the respective work function. Acidic treatment leads to protonation of the ITO surface and an interfacial dipole pointing away from the electrode is formed with the anions, leading to an increase of the work function of the electrode. Basic treatment forms an interfacial dipole which points towards the electrode and the work function is reduced. Large counterions result in a larger surface dipole and thus shift the work function more effectively.[142]

Photoelectron spectroscopy was used to quantify the influence of various acid and base treatments of the ITO surface (Fig. 17). The work function of untreated ITO was measured at 4.4 eV and remained unchanged when the electrodes were dipped in water (neutral pH). Acidic treatment with nitric acid, hexafluorophosphoric acid and phosphoric acid increased the work function up to 5.1 eV, basic treatment with sodium hydroxide and tetrabutylammonium hydroxide decreased the work function by 0.2 and 0.5 eV, respectively.

3.3.1 Self-assembled monolayers (SAMs). The modification of the electrode work function in OPV devices to adjust the barrier height between two layers by SAMs, *i.e.* active layer/interfacial layer/electrode, was successfully reported in several publications.[145,147] The strength and direction of the dipole determine the resulting work function of the SAM modified substrate and the interface. An adjusted barrier results in improved device performance, a non-adjusted barrier in decreased device performance. Several groups investigated the impact of a variety of SAMs to the work function of the

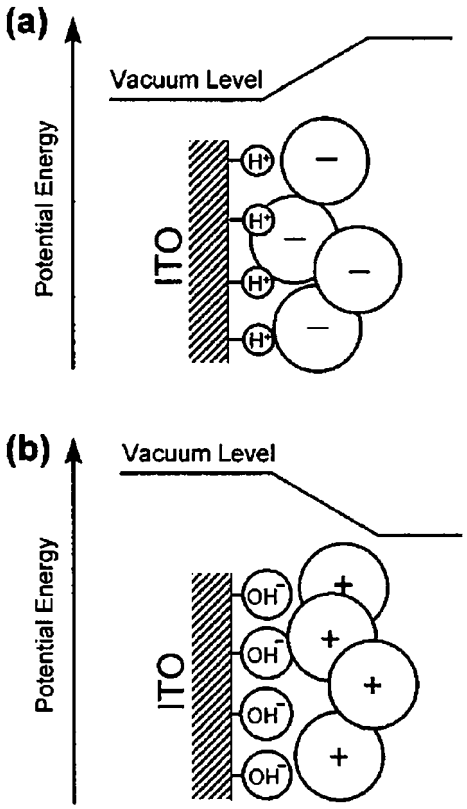

Fig. 16 Schematic illustration of the monolayer adsorption of Bronsted acids (a) and bases (b) onto the ITO surface. The corresponding qualitative vacuum level shift is also indicated in the graph. Adapted with permission from ref. 142. Copyright 1999 American Institute of Physics.

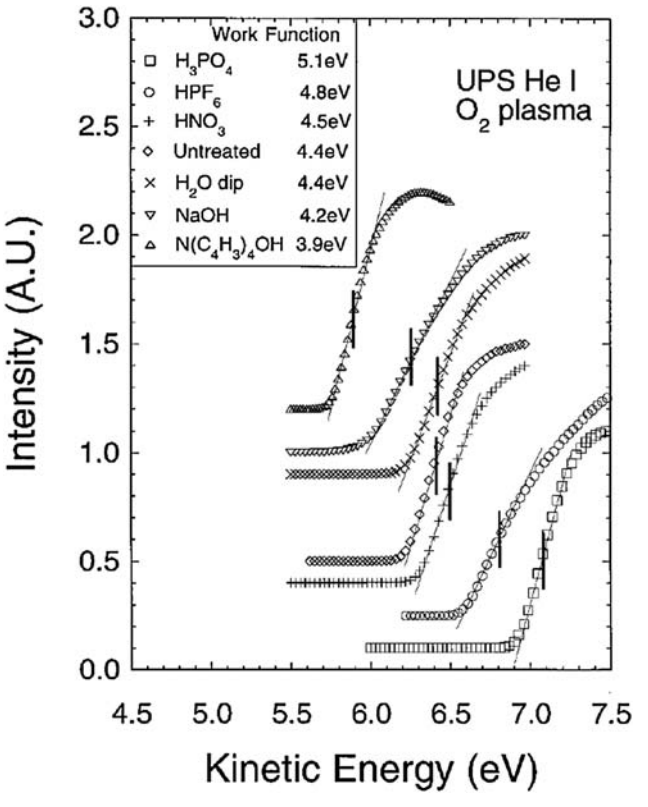

Fig. 17 He I UPS spectrum of ITO taken with 25.000 V bias applied to the sample. The inelastic cutoff part of the electron energy distribution curve is shown. Different surface treatments as well as the corresponding work functions are indicated in the graph. Adapted with permission from ref. 142. Copyright 1999, American Institute of Physics.

electrodes, the interface electrode/interfacial layer and interfacial layer/active layer as well as the resulting device performance.

The modification of the work function of ITO by 4-chlorobenzoylchloride (CBC), 4-chlorobenzenesulfonyl chloride (CBS) and 4-chlorophenyldichlorophosphate (CBP)[143] as well as with SAMs with a terminal group of $–NH_2$, $–CH_3$ and $–CF_3$[144] results in improved device performance. The metal/SAM/ZnO interface was modified with lauric acid, mercaptoundecanoic acid and perfluorotetradecanoic acid.[145] Similarly, the interface between TiOx and P3HT:PCBM was modified with lauric acid, benzoic acid, terthiophene and C_{60} substituted benzoic acid.[146]

Yip *et al.*[147] modified the interface ZnO/metal electrode by a series of para-substituted benzoic acid (BA–X) SAMs with negative ($–OCH_3$, $–CH_3$, –H) and positive (–SH, $–CF_3$, –CN) dipoles. The gas-phase dipole moment (D) of BA–X is $–OCH_3$ (-3.9 D) < $–CH_3$ (-2.9 D) < –H (-2.0 D) < –SH (1.5 D) < $–CF_3$ (2.1 D) < –CN (3.7 D). Table 3 summarizes results for the device structure ITO/Pedot:PSS/P3HT:PCBM/ZnO/BA-X/Al.

SAMs with a positive dipole moment increase the barrier height between ZnO and Al resulting in a decrease in device performance. SAMs with a negative dipole show a positive effect to the device performance and the PCE increases from 3.16% for –/ZnO/Al to 4.21% for –/ZnO/BA–OCH_3/Al. The device performance correlates with the strength of the dipole and the one with the highest dipole has the best performance. The authors present successfully that the right choice of SAMs improves the device performance and makes varying metal electrode materials suitable for OPV.[147]

Table 3 Summary of device performance of polymer solar cells with different benzoic-acid-based molecules modified ZnO/Al cathodes. Adapted with permission from ref. 147. Copyright 2008, Wiley VCH

Cathode configuration	Voc/ V	Jsc/ mA cm^{-2}	FF	PCE [%]	Rp [Ω cm^2]	Rs [Ω cm^2]
ZnO/BA–OCH_3/Al	0.65	11.61	0.55	4.21	648.8	1.5
ZnO/BA–CH_3/Al	0.64	11.63	0.49	3.63	438.0	2.1
ZnO/BA–H/Al	0.64	11.46	0.48	3.48	583.3	2.2
ZnO/Al	0.6	11.29	0.47	3.16	392.5	3.1
ZnO/BA–SH/Al	0.45	10.44	0.42	1.95	184.7	13.3
ZnO/BA–CF_3/Al	0.3	8.97	0.31	0.84	64.1	24.2
ZnO/BA–CN/Al	0.27	8.15	0.28	0.62	47.2	14.4

3.3.2 Salts. The most prominent approaches for improving the device performance of OPV cells make use of the salts LiF and Cs_2CO_3. Especially for LiF two possible origins of the improvement in PCE are under discussion: doping of the acceptor material by Li and modification of the work function of the electrode through dipole formation.[148–153]

For the normal structure a prominent cathode is a combination of LiF and Al, both of which are thermally evaporated on top of the active layer. The incorporation of a 0.6 nm thick LiF layer between the active layer and the Al electrode does improve

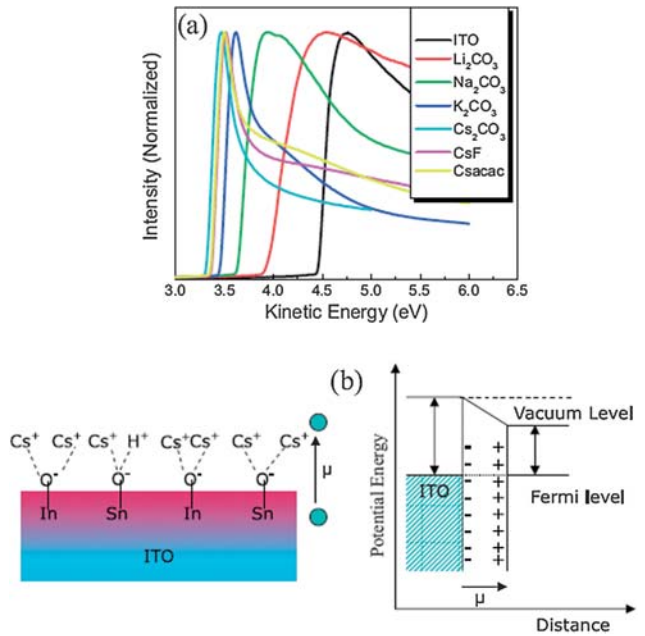

Fig. 18 a) Evolution of secondary electron edge with different buffer layers on ITO, b) scheme for the formation of dipole layer on ITO. Adapted with permission from ref. 158. Copyright 2008, Wiley VCH.

the FF from 53% to 63% and Voc from 0.76V to 0.83V for a MDMO-PPV/PCBM solar cell. Even LiF/Au can act as cathode despite the high work function of Au of 5.1 eV.[148] LiF was first applied in OLEDs in the structure tris(8-hydroxyquinoline)aluminium (Alq_3)/LiF/Al. It was suggested that the decomposition of LiF leads to chemical doping of Alq_3 by Li.[154] Li^+ ions diffuse into and dope the organic layer. On the one hand this effect is favorable since it allows doping of the active layer by placing the dopant on top of the active layer. On the other hand the diffusing dopant limits the lifetime.[155] Cs, also a dopant for organic materials, has a lower diffusivity than Li and promises a higher lifetime.[155] Similar results are reported for doping of bathophenanthroline (BPhen) and BCP.[156,157]

Cs_2CO_3 is an example of a solution deposited salt. The work functions of ITO coated with different salts are depicted in Fig. 18 and decreases from ITO to ITO/CS_2CO_3. Voc and Isc increases with the reduction of the work function of the cathode. Voc increases from 0.2 V to 0.56 V and Isc from 7.01 mA cm^{-2} to 9.7 mA cm^{-2} when applying a Cs_2CO_3 layer on ITO. Fig. 18(b) schematically presents the O–Cs dipole formed which results in a reduction of the work function of the coated ITO.[158]

This trend holds when reducing the work function of ITO/CS_2CO_3 further from 3.45 eV to 3.06 eV by an annealing step at 150 °C. The reduced work function results in an improvement in PCE from 2.31% to 4.19%. Voc is improved from 0.55 V to 0.59 V, Jsc from 7.61 mA cm^{-2} to 11.13 mA cm^{-2} and the FF from 55 to 64%.[159]

4 Summary

In conclusion we discussed the impact of interfacial layers on the performance of organic solar cells and reviewed a wide range of materials applied for OPV. We distinguished between metallic, organic, inorganic, semiconducting, n-type and p-type interfacial layers and reviewed the most prominent ones. For the development of future OPV structures with increased PCE and lifetime, the right choice of interface materials will be essential. Many groups demonstrated that improved interfaces are essential for optimized PCE. An excellent interface material is not only characterized by the resulting PCE of the device, but also by the degradation of the interfacial layer itself and the degradation in combination with the other materials of the OPV cell. The optimization of both PCE and lifetime will further improve the potential and attractiveness of OPV. The optimum choice of interface materials is a key factor for highly efficient and stable OPV devices.

References

1 W. Y. Wong, X. Z. Wang, Z. He, A. B. Djurisic, C. T. Yip, K. Y. Cheung, H. Wang, C. S. K. Mak and W. K. Chan, *Nat. Mater.*, 2007, **6**, 521.
2 J. Peet, J. Y. Kim, N. E. Coates, W. L. Ma, D. Moses, A. J. Heeger and G. C. Bazan, *Nat. Mater.*, 2007, **6**, 497.
3 P. W. M. Blom, V. D. Mihailetchi, L. J. A. Koster and D. E. Markov, *Adv. Mater.*, 2007, **19**, 1551.
4 See Solarmer press release 2009, www.solarmer.com.
5 See Konarka press release 2008, www.konarka.com.
6 J. Y. Kim, K. Lee, N. E. Coates, D. Moses, T. Q. Nguyen, M. Dante and A. J. Heeger, *Science*, 2007, **317**, 222.
7 G. K. Mor, K. Shankar, M. Paulose, O. K. Varghese and C. A. Grimes, *Appl. Phys. Lett.*, 2007, **91**, 152111.
8 R. Steim, S. A. Choulis, P. Schilinsky and C. J. Brabec, *Appl. Phys. Lett.*, 2008, **92**, 093303.
9 H.-H. Liao, L.-M. Chen, Z. Xu, G. Li and Y. Yang, *Appl. Phys. Lett.*, 2008, **92**, 173303.
10 J. A. Hauch, P. Schilinsky, S. A. Choulis, S. Rajoelson and C. J. Brabec, *Appl. Phys. Lett.*, 2008, **93**, 103306.
11 C. J. Brabec, N. S. Sariciftci and J. C. Hummelen, *Adv. Funct. Mater.*, 2001, **11**, 15.
12 M. Lenes, G.-J. A. H. Wetzelaer, F. B. Kooistra, S. C. Veenstra, J. C. Hummelen and P. W. M. Blom, *Adv. Mater.*, 2008, **20**, 2116–2119.
13 D. Mühlbacher, M. Scharber, M. Morana, Z. Zhu, D. Waller, R. Gaudiana and C. Brabec, *Adv. Mater.*, 2006, **18**, 2884–2889.
14 J. Peet, J. Y. Kim, N. E. Coates, W. L. Ma, D. Moses, A. J. Heeger and G. C. Bazan, *Nat. Mater.*, 2007, **6**, 497–500.
15 J. Hou, H. Y. Chen, S. Zhang, G. Li and Y. Yang, *J. Am. Chem. Soc.*, 2008, **130**, 16144–16145.
16 H.-H. Liao, L.-M. Chen, Z. Xu, G. Li and Y. Yang, *Appl. Phys. Lett.*, 2008, **92**, 173303.
17 L. M. Chen, Z. Hong, G. Li and Y. Yang, *Adv. Mater.*, 2009, **21**, 1434–1449.
18 G. Li, C.-W. Chu, V. Shrotriya, J. Huang and Y. Yang, *Appl. Phys. Lett.*, 2006, **88**, 253503.
19 P. W. M. Blom, V. D. Mihailetchi, L. J. A. Koster and D. E. Markov, Device Physics of Polymer : Fullerene Bulk Heterojunction Solar Cells, *Adv. Mater.*, 2007, **19**, 1551–1566.
20 W. Osikowicz, M. P. de Jong and W. R. Salaneck, *Adv. Mater.*, 2007, **19**, 4213.
21 A. Crispin, X. Crispin, M. Fahlman, M. Berggren and W. R. Salaneck, *Appl. Phys. Lett.*, 2006, **89**, 213503.
22 S. Braun, W. R. Salaneck and M. Fahlman, *Adv. Mater.*, 2009, **21**, 1450.
23 C. D. Lindstrom and X.-Y. Zhu, *Chem. Rev.*, 2006, **106**, 4281.
24 X. Crispin, V. Geskin, A. Crispin, J. Cornil, R. Lazzaroni, W. R. Salaneck and J. L. J. Bredas, *J. Am. Chem. Soc.*, 2002, **124**, 8131.
25 H. Ishii, K. Sugiyama, E. Ito and K. Seki, *Adv. Mater.*, 1999, **11**, 605.
26 V. D. Mihailetchi, P. W. M. Blom, J. C. Hummelen and M. T. Rispens, *J. Appl. Phys.*, 2003, **94**, 6849.
27 C. J. Brabec, A. Cravino, D. Meissner, N. S. Sariciftci, T. Fromherz, M. T. Rispens, L. Sanchez and J. C. Hummelen, *Adv. Funct. Mater.*, 2001, **11**, 374.

28 M. C. Scharber, D. Mühlbacher, M. Koppe, P. Denk, C. Waldauf, A. J. Heeger and C. J. Brabec, *Adv. Mater.*, 2006, **18**, 789.
29 A. Cravino, *Appl. Phys. Lett.*, 2007, **91**, 243502.
30 M. Campoy-Quiles, T. Ferenczi, T. Agostinelli, P. G. Etchegoin, Y. Kim, T. D. Anthopoulos, P. N. Stavrinou, D. D. C. Bradley and J. Nelson, *Nat. Mater.*, 2008, **7**, 158.
31 Z. Xu, L.-M. Chen, G. Yang, C.-H. Huang, J. Hou, Y. Wu, G. Li, C.-S. Hsu and Y. Yang, *Adv. Funct. Mater.*, 2009, **19**, 1227–1234.
32 Waldauf, M. Morana, P. Denk, P. Schilinsky, K. Coakley, S. A. Choulis and C. J. Brabec, *Appl. Phys. Lett.*, 2006, **89**, 233517.
33 X. L. Chen, B. H. Xu, J. M. Xue, Y. Zhao, C. C. Wei, J. Sun, Y. Wang, X. D. Zhang and X. H. Geng, *Thin Solid Films*, 2007, **515**, 3753–3759.
34 V. Bhosle, J. T. Prater, Fan Yang, D. Burk, S. R. Forrest and J. Narayan, *J. Appl. Phys.*, 2007, **102**, 023501.
35 J. Owen, M. S. Som, K.-H. Yoo, B. D. Ahn and S. Y. Lee, *Appl. Phys. Lett.*, 2007, **90**, 033512.
36 Y. Yamamoto, K. Saito, K. Takahashi and M. Konagai, *Sol. Energy Mater. Sol. Cells*, 2001, **65**, 125.
37 S. Park, S. J. Tark, J. S. Lee, H. Lim and D. Kim, *Sol. Energy Mater. Sol. Cells*, 2009, **93**(6–7), 1020–1023.
38 O. Kluth, B. Rech, L. Hoben, S. Wieder, G. Schöpe, C. Beneking, H. Wagner and A. Löffl, *Thin Solid Films*, 1999, **351**, 247.
39 M. W. Rowell, M. A. Topinka, M. D. McGehee, H. J. Prall, G. Dennler, N. S. Sariciftci, L. B. Hu and G. Gruner, *Appl. Phys. Lett.*, 2006, **88**, 233506.
40 G. Eda, Y. Y. Lin, S. Miller, C. W. Chen, W. F. Su and M. Chhowalla, *Appl. Phys. Lett.*, 2008, **92**, 233305.
41 Y. H. Zhou, F. L. Zhang, K. Tvingstedt, S. Barrau, F. H. Li, W. J. Tian and O. Inganas, *Appl. Phys. Lett.*, 2008, **92**, 233308.
42 K. Tvingstedt and O. Inganäs, *Adv. Mater.*, 2007, **19**, 2893–2897.
43 J. Y. Lee, S. T. Connor, Y. Cui and P. Peumans, *Nano Lett.*, 2008, **8**, 689–692.
44 B. O'Connor, C. Haughn, K. H. An, K. P. Pipe and M. Shtein, *Appl. Phys. Lett.*, 2008, **93**, 223304.
45 C. Guillen and J. Herrero, *Sol. Energy Mater. Sol. Cells*, 2008, **92**, 938–941.
46 B. V. Andersson, D. M. Huang, H. J. Moulé and O. Inganäs, *Appl. Phys. Lett.*, 2009, **94**, 043302.
47 J. Y. Kim, S. H. Kim, H. H. Lee, K. Lee, W. Ma, X. Gong and A. J. Heeger, *Adv. Mater.*, 2006, **18**, 572.
48 A. Roy, S. H. Park, S. Cowan, M. H. Tong, S. Cho, K. Lee and A. J. Heeger, *Appl. Phys. Lett.*, 2009, **95**, 013302.
49 S. H. Park, A. Roy, S. Beaupre, S. Cho, N. Coates, J. S. Moon, D. Moses, M. Leclerc, K. Lee and A. J. Heeger, *Nat. Photonics*, 2009, **3**, 297.
50 K. Suemori, M. Yokoyama and M. Hiramoto, *J. Appl. Phys.*, 2006, **99**, 036109.
51 M. O. Reese, A. J. Morfa, M. S. White, N. Kopidakis, S. E. Shaheen, G. Rumbles and D. S. Ginley, *Sol. Energy Mater. Sol. Cells*, 2008, **92**, 746–752.
52 S. T. Lee, Z. Q. Gao and L. S. Hung, *Appl. Phys. Lett.*, 1999, **75**, 10.
53 K. Lee, J. Y. Kim, S. H. Park, S. H. Kim, S. Cho and A. J. Heeger, *Adv. Mater.*, 2007, **19**, 2445.
54 M. D. Irwin, B. Buchholz, A. W. Hains, R. P. H. Chang and T. J. Marks, *Proc. Natl. Acad. Sci. U. S. A.*, 2008, **105**, 2783–2787.
55 A. R. Schlatmann, D. Wilms Floet, A. Hilberer, F. Garten, P. J. M. Smulders, J. M. Klapwijk and G. Hadziioannou, *Appl. Phys. Lett.*, 1996, **69**, 1764.
56 P. Peumans and S. R. Forrest, *Appl. Phys. Lett.*, 2001, **79**, 126.
57 Y. Hirose, A. Kahn, V. Aristov, P. Soukiassian, V. Bulović and S. R. Forrest, *Phys. Rev. B: Condens. Matter*, 1996, **54**, 13748.
58 P. Peumans, V. Bulovic and S. R. Forrest, *Appl. Phys. Lett.*, 2000, **76**, 2650.
59 J. Blochwitz, M. Pfeiffer, T. Fritz and K. Leo, *Appl. Phys. Lett.*, 1998, **73**, 729.
60 W. Gao and A. Kahn, *Org. Electron.*, 2002, **3**, 53.
61 W. Gao and A. Kahn, *J. Appl. Phys.*, 2003, **94**, 359.
62 C. K. Chan, F. Amy, Q. Zhang, S. Barlow, S. Marder and A. Kahn, *Chem. Phys. Lett.*, 2006, **431**, 67.
63 C. K. Chan, W. Zhao, S. Barlow, S. Marder and A. Kahn, *Org. Electron.*, 2008, **9**, 575.
64 Steven K. Hau, Hin-Lap Yip, Kirsty Leong and Alex K.-Y. Jen, *Org. Electron.*, 2009, **10**(4), 719–723.
65 Jung-Yong Lee, Stephen T. Connor, Yi Cui and Peter Peumans, *Nano Lett.*, 2008, **8**(2), 689–692.
66 M. O. Reese, M. S. White, G. Rumbles, D. S. Ginley and S. E. Shaheen, *Appl. Phys. Lett.*, 2008, **92**, 053307.
67 Herbert B. Michaelson, *J. Appl. Phys.*, 1977, **48**(11), 4729.
68 M. Chikamatsu, T. Taima, Y. Yoshida, K. Saito and K. Yase, *Appl. Phys. Lett.*, 2004, **84**, 127.
69 A. Colsmann, *Ladungstransportschichten für effiziente organische Halbleiterbauelemente*, Universitätsverlag Karlsruhe, 2009, 978-3-86644-332-7.
70 C. Tao, S. Ruan, G. Xie, X. Kong, L. Shen, F. Meng, C. Liu, X. Zhang, W. Dong and W. Chen, *Appl. Phys. Lett.*, 2009, **94**, 043311.
71 M. Y. Chan, C. S. Lee, S. L. Lai, M. K. Fung, F. L. Wong, H. Y. Sun, K. M. Lau and S. T. Lee, *Appl. Phys. Lett.*, 2006, **100**, 094506.
72 S. Han, W. S. Shin, M. Seo, D. Gupta, S.-J. Moon and S. Yoo, *Org. Electron.*, 2009, **10**, 791, DOI: 10.1016/j.orgel.2009.03.016.
73 V. Shrotriya, G. Li, Y. Y. Yao, C. W. Chu and Y. Yang, *Appl. Phys. Lett.*, 2006, **88**, 073508.
74 K. Takanezawa, K. Tajima and K. Hashimoto, *Appl. Phys. Lett.*, 2008, **93**, 063308.
75 J. S. Huang, C. Y. Chou, M. Y. Liu, K. H. Tsai, W. H. Li and C. F. Lin, *Org. Electron.*, 2009, **10**, 1060–1065.
76 H.-H. Liao, L.-M. Chen, Z. Xu, G. Li and Y. Yang, *Appl. Phys. Lett.*, 2008, **92**, 173303.
77 A. K. K. Kyaw, X. W. Sun, C. Y. Jiang, G. Q. Lo, D. W. Zhao and D. L. Kwong, *Appl. Phys. Lett.*, 2008, **93**, 221107.
78 L. Cattin, F. Dahou, Y. Lare, M. Morsli, R. Tricot, S. Houari, A. Mokrani, K. Jondo, A. Khelil, K. Napo and J. C. Bernède, *J. Appl. Phys.*, 2009, **105**, 034507.
79 S. Han, W. S. Shin, M. Seo, D. Gupta, S.-J. Moon and S. Yoo, *Org. Electron.*, 2009, **10**, 791, DOI: 10.1016/j.orgel.2009.03.016.
80 R. Steim, S. A. Choulis, P. Schilinsky and C. J. Brabec, *Appl. Phys. Lett.*, 2008, **92**, 093303.
81 A. Hayakawa, O. Yoshikawa, T. Fujieda, K. Uehara and S. Yoshikawa, *Appl. Phys. Lett.*, 2007, **90**, 163517.
82 G. K. Mor, K. Shankar, M. Paulose, O. K. Varghese and C. A. Grimes, *Appl. Phys. Lett.*, 2007, **91**, 152111.
83 M. N. M. Glatthaar, B. Zimmermann, P. Lewer, M. Riede, A. Hinsch and J. Luther, *Thin Solid Films*, 2005, **491**, 298.
84 J. Gilot, I. Barbu, M. M. Wienk and R. A. J. Janssen, *Appl. Phys. Lett.*, 2007, **91**, 113520.
85 M. S. White, D. C. Olson, S. E. Shaheen, N. Kopidakis and D. S. Ginley, *Appl. Phys. Lett.*, 2006, **89**, 143517.
86 L. Vayssieres, *Adv. Mater.*, 2003, **15**, 464.
87 S. K. Hau, H.-L. Yip, N. S. Baek, J. Zou, K. O'Malley and A. K.-Y. Jen, *Appl. Phys. Lett.*, 2008, **92**, 253301.
88 T. Kuwabara, H. Sugiyama, T. Yamaguchi and K. Takahashi, *Thin Solid Films*, 2009, **517**(13), 3766–3769.
89 K. Takanezawa, K. Tajima and K. Hashimoto, *Appl. Phys. Lett.*, 2008, **93**, 063308.
90 J. S. Huang, C. Y. Chou, M. Y. Liu, K. H. Tsai, W. H. Lin and C. F. Lin, *Org. Electron.*, 2009, **10**, 1060–1065.
91 K. Takanezawa, K. Hirota, Q. S. Wei, K. Tajima and K. Hashimoto, *J. Phys. Chem.*, 2007, **C111**, 7218–7223.
92 I. Gonzallez-Valls and M. Lira-Cantu, *Energy Environ. Sci.*, 2009, **2**, 19–34.
93 D. C. Olson, J. Piris, R. T. Collins, S. E. Shaheen and D. S. Ginley, *Thin Solid Films*, 2006, **496**, 26.
94 W. H. Baek, I. Seo, T. S. Yoon, H. H. Lee, C. M. Yun and Y. S. Kim, *Sol. Energy Mater. Sol. Cells*, 2009, **93**, 1587–1591.
95 G. K. Mor, K. Shankar, M. Paulose, O. K. Varghese and C. A. Grimes, *Appl. Phys. Lett.*, 2007, **91**, 152111.
96 M. Nada, T. Gonda, Q. Shen, H. Shimada, T. Toyoda and N. Kobayashi, *Jpn. J. Appl. Phys.*, 2009, **48**, 025505.
97 M. H. Park, J. H. Li, A. Kumar, G. Li and Y. Yang, *Adv. Funct. Mater.*, 2009, **19**, 1241–1246.
98 A. A. Zakhidov, J. K. Lee, H. H. Fong, J. A. DeFranco, M. Chatzichristidi, P. G. Taylor, C. K. Ober and G. G. Malliaras, *Adv. Mater.*, 2008, **20**, 3481–3484.
99 A. Kumar, G. Li, Z. Hong and Y. Yang, *Nanotechnology*, 2009, **20**, 165202.
100 K. Walzer, B. Maennig, M. Pfeiffer and K. Leo, *Chem. Rev.*, 2007, **107**, 1233–1271.

101 S. E. Saheen, C. J. Brabec, N. S. Sariciftci, F. Padinger, T. Fromberz and J. C. Hummelen, *Appl. Phys. Lett.*, 2001, **78**, 841.
102 Y. Cao, G. Yu, C. Zhang, R. Menon and A. J. Heeger, *Synth. Met.*, 1997, **87**, 171.
103 S. A. Carter, M. Angelopoulos, S. Karg, P. J. Brock and J. C. Scott, *Appl. Phys. Lett.*, 1997, **70**, 2067.
104 J. C. Carter, I. Grizzi, S. K. Heeks, D. J. Lacey, S. G. Latham, P. G. May, O. R. d. l. Panos, K. Pichler, C. R. Towns and H. F. Wittman, *Appl. Phys. Lett.*, 1997, **71**, 34.
105 C. Y. Li, T. C. Wen, T. H. Lee, T. F. Guo, J. C. A. Huang, Y. C. Lin and Y. J. Hsu, *J. Mater. Chem.*, 2009, **19**, 1643.
106 C. Y. Li, T. C. Wen, T. F. Guo and S. S. Hou, *Polymer*, 2008, **49**, 957.
107 G. Gustafsson, Y. Cao, G. M. Treacy, F. Klavetter, N. Colaneri and A. J. Heeger, *Nature*, 1992, **357**, 477.
108 Y. Yang and A. J. Heeger, *Appl. Phys. Lett.*, 1994, **64**, 1245.
109 J. Jang, J. Ha and K. Kim, *Thin Solid Films*, 2008, **516**, 3152.
110 Y. Kim, A. M. Ballantyne, J. Nelson and D. D. C. Bradley, *Org. Electron.*, 2009, **10**, 205–209.
111 C. J. Ko, Y. K. Lin, F. C. Chen and C. W. Chu, *Appl. Phys. Lett.*, 2007, **90**, 063509.
112 D. Bagchi and R. Menon, *Chem. Phys. Lett.*, 2006, **425**, 114.
113 H. J. Snaith, H. Kenrick, M. Chiesa and R. H. Friend, *Polymer*, 2005, **46**, 2573.
114 S. Timpanaro, M. Kemerink, F. J. Touwslager, M. M. De Koc and S. Schrader, *Chem. Phys. Lett.*, 2004, **394**, 339.
115 S. Ashizawa, R. Horikawa and H. Okuzaki, *Synth. Met.*, 2005, **153**, 5.
116 L. A. A. Pettersson, S. Ghosh and O. Inganäs, *Org. Electron.*, 2002, **3**, 143.
117 S. Ghosh and O. Inganäs, *Synth. Met.*, 2001, **121**, 1321.
118 S. K. M. Jönsson, J. Birgerson, X. Crispin, G. Greezynski, W. Osikowicz, A. W. D. van der Gon, W. R. Salaneck and M. Fahlman, *Synth. Met.*, 2003, **139**, 1.
119 F. Zhang, M. Joansson, M. R. Andersson, J. C. Hummelen and O. Inganäs, *Adv. Mater.*, 2002, **14**, 662.
120 X. Crispin, S. Marciniak, W. Osikowicz, G. Zotti, A. W. Denier van der Gon, F. Louwet, M. Fahlman, L. Groenendaal, F. de Schryver and W. R. Salaneck, *J. Polym. Sci., Part B: Polym. Phys.*, 2003, **41**, 2561.
121 J. Ouyang, C. W. Chu, F. C. Chen, Q. Xu and Y. Yang, *Adv. Funct. Mater.*, 2005, **15**, 203.
122 J. Y. Kim, J. H. Jung, D. E. Lee and J. Joo, *Synth. Met.*, 2002, **126**, 311.
123 J. H. Huang, D. Kekuda, C. W. Chu and K. C. Ho, *J. Mater. Chem.*, 2009, **19**, 3704–3712.
124 T. Aernouts, P. Vanlaeke, W. Geens, J. Poortmans, P. Heremans, S. Borghs, R. Mertens, R. Andriessen and L. Leenders, *Thin Solid Films*, 2004, **451–452**, 22.
125 M. Glatthaar, M. Niggemann, B. Zimmermann, P. Lewer, M. Riede, A. Hinsch and J. Luther, *Thin Solid Films*, 2005, **491**, 298.
126 K. Tvingstedt and O. Inganäs, *Adv. Mater.*, 2007, **19**, 2893.
127 M. P. de Jong, L. J. van IJzendoorn and M. J. A. de Voigt, *Appl. Phys. Lett.*, 2000, **77**, 2255.
128 M. Jorgensen, K. Norrman and F. C. Krebs, Stability/degradation of polymer solar cells, *Sol. Energy Mater. Sol. Cells*, 2008, **92**, 686–714.
129 E. Vitoratos, S. Sakkopoulos, E. Dalas, N. Paliatsas, D. Karageorgopoulos, F. Petraki, S. Kennou and S. A. Choulis, *Org. Electron.*, 2009, **10**, 61.
130 J.-S. Kim, P. K. H. Ho, C. E. Murphy, N. Baynes and R. H. Friend, *Adv. Mater.*, 2002, **14**, 206.
131 J. Huang, M. Pfeiffer, A. Werner, J. Blochwitz, K. Leo and S. Liu, Low voltage organic electroluminescent devices using pin-structures, *Appl. Phys. Lett.*, 2002, **80**(1), 139.
132 J. Xue, S. Uchida, B. P. Rand and S. R. Forrest, *Appl. Phys. Lett.*, 2004, **85**, 5757.
133 M. Vogel, S. Doka, Ch. Breyer, M. Ch. Lux-Steiner and K. Fostiropoulos, *Appl. Phys. Lett.*, 2006, **89**, 163501.
134 A. G. Werner, F. Li, K. Harada, M. Pfeiffer, T. Fritz and K. Leo, *Appl. Phys. Lett.*, 2003, **82**, 4495.
135 A. G. Werner, F. Li, K. Harada, M. Pfeiffer, T. Fritz, K. Leo and S. Machill, *Adv. Funct. Mater.*, 2004, **14**, 255.
136 F. Li, M. Pfeiffer, A. Werner, K. Harada and K. Leo, *J. Appl. Phys.*, 2006, **100**, 023716.
137 F. Li, A. G. Werner, M. Pfeiffer and K. Leo, *J. Phys. Chem. B*, 2004, **108**, 17076.
138 B. Maenning, J. Drechsel, D. Gebeyehu, P. Simon, F. Kozlowski, A. Werner, F. Li, S. Grundmann, S. Sonntag, M. Koch, K. Leo, M. Pfeiffer, H. Hoppe, D. Meissner, N. S. Sariciftci, I. Riedel, V. Dyakonov and J. Parisi, *Appl. Phys. A: Mater. Sci. Process.*, 2004, **79**, 1.
139 J. Drechsel, B. Maenning, F. Kozlowski, M. Pfeiffer, K. Leo and H. Hoppe, *Appl. Phys. Lett.*, 2005, **86**, 244102.
140 M. Y. Chan, S. L. Lai, K. M. Lau, C. S. Lee and S. T. Lee, *Appl. Phys. Lett.*, 2006, **89**, 163515.
141 C. K. Chan, W. Zhao, A. Kahn and I. G. Hill, *Appl. Phys. Lett.*, 2009, **94**, 203306.
142 F. Nüesch, L. J. Rothberg, E. W. Forsythe, Quoc Toan Le and Yongli Gao, *Appl. Phys. Lett.*, 1998, **74**, 34.
143 S. Khodabakhsh, B. M Sanderson, J. Nelson and T. S Jones, *Adv. Funct. Mater.*, 2006, **16**, 95–100.
144 J. S. Kim, J. H. Park, J. H. Lee, J. Jo, D. Kim and K. Cho, *Appl. Phys. Lett.*, 2007, **91**, 112111–3.
145 H. L. Yip, S. K. Hau, N. S. Baek, H. Ma and A. K. Y. Jen, *Appl. Phys. Lett.*, 2008, **92**, 193313.
146 S. K. Hau, H. L. Yip, O. Acton, N. S. Baek, H. Ma and A. K. Y. Jen, *J. Mater. Chem.*, 2008, **18**, 5113–5119.
147 H. L. Yip, S. K. Hau, N. S. Baek, H. Ma and A. K. Y. Jen, *Adv. Mater.*, 2008, **20**, 2376.
148 C. J. Brabec, S. E. Shaheen, C. Winder, N. S. Sariciftci and P. Denk, *Appl. Phys. Lett.*, 2002, **80**, 1288.
149 S. K. M. Jonsson, E. Carlegrim, F. Zhang, W. R. Salaneck and M. Fahlman, *Jpn. J. Appl. Phys.*, 2005, **44**, 3695.
150 T. M. Brown, R. H. Friend, I. S. Millard, D. J. Lacey, J. H. Burroughes and F. Cacialli, *Appl. Phys. Lett.*, 2000, **77**, 3096.
151 L. S. Hung, C. W. Tang and M. G. Mason, *Appl. Phys. Lett.*, 1997, **70**, 152.
152 S. E. Shaheen, G. E. Jabbour, M. M. Morrell, Y. Kawabe, B. Kippelen, N. Peyghambarian, M. F. Nabor, R. Schlaf, E. A. Mash and N. R. Armstron, *J. Appl. Phys.*, 1998, **84**, 2324.
153 M. Matsumura, K. Furukawa and Y. Jinde, *Thin Solid Films*, 1998, **331**, 96.
154 D. Grozea, A. Turak, X. D. Feng, Z. H. Lu, D. Johnson and R. Wood, *Appl. Phys. Lett.*, 2002, **81**, 3173.
155 J. Kido and T. Matsumoto, *Appl. Phys. Lett.*, 1998, **73**, 2866.
156 J. Huang, M. Pfeiffer, A. Werner, J. Blochwitz, K. Leo and S. Liu, *Appl. Phys. Lett.*, 2002, **80**(1), 139.
157 G. Parthasarathy, C. Shen, A. Kahn and S. R. Forrest, *J. Appl. Phys.*, 2001, **89**, 4986.
158 J. Huang, G. Li and Y. Yang, *Adv. Mater.*, 2008, **20**, 415–419.
159 H. H. Liao, L. M. Chen, Z. Xu, G. Li and Y. Yang, *Appl. Phys. Lett.*, 2008, **92**, 173303.

